Carpathian Journal of Earth and Environmental Sciences, May 2015, Vol. 10, No. 2, p. 45 - 58

MULTI-PHASED NORMAL FAULTING OF THE EISENSTADT-SOPRON BASIN MARGINS AS A CONTROLLING FACTOR OVER SPATIALLY CONFINED COAL MINI-HYDROCARBON PLAY (EAST AUSTRIA)

Darko SPAHIĆ[1,*] & Ljupko RUNDIĆ[2]

[1]*Schlumberger * Corresponding Author. Address: Leningradskoe shosse 16A, build.3, 125171, Moscow, Russian Federation.E-mail: DSpahic@slb.com, / darkogeo2002@hotmail.com; Tel.: + 7 495 825 8200 ext 602737.*

[2]*University of Belgrade, Faculty of Mining and Geology, Department of Regional Geology, Kamenička 6, 11000, Belgrade, Serbia E-mail:ljupko.rundic@rgf.bg.ac.rs*

Abstract: The deformation chronology of the margins of the south-eastern and north-western Eisenstadt–Sopron sub-basin, initially (i) the multiphase normal faulting convergence with the sediment stacking, tectonic inversion and eroded rock volumes were characterised and subsequently (ii) the effects of these processes on the local, spatially confined coal bearing mini-petroleum system were additionally reproduced and quantified. The deformations in the south-eastern margin of the Basin indicated a late Sarmatian - Pannonian development of fault-adjacent reverse drag as potentially the main trap formation time. A combination of 'palaeo' and 'present day heat flow scenarios was used for the calculation of hydrocarbon generation within the north-western depocentre accommodated by the initial early Tertiary syn-rift stretching and syn-sedimentary deposition associated with the Forchenstein fault. According to a palinspastic analysis, deformation chronology and thermal basin models, hydrocarbon generation commenced during the Middle Miocene at about 14 Ma and terminated during the Late Miocene (≈ 10 Ma) due to a rapid cooling caused by uplift and erosion. Over 50% of the total resource potential was realized at the deepest mini-basin section. The results of 1D basin modelling of the north-western mini-basin depocentre suggested that there is a high probability of once active source rocks around a depocentre, however with limited generation volumes.

Keywords: Eisenstadt–Sopron, coal mini-play, geomechanical-based restoration, basin modelling, heat flow, footwall traps.

1. INTRODUCTION

Eisenstadt–Sopron (ES) sub-basin (Fig. 1a) presents the eastern margin of the main Vienna Basin. The main Vienna Basin contains over 3500 wells (Hamilton et al., 2000), whereby the Austrian parts of the Styrian and Pannonian Basin have ca. 50 wells. In Austria, 108.5 MM tonnes/oil (c.752 MMBO) and 72.1 Bm^3 gas (c.2.7TCF) have been produced; 99.5 MM tonnes/oil (c.700 MMBO) and 52.4 Bm^3 gas (c.2.0TCF) from the Austrian part of the Vienna Basin. However, the Pannonian and Styrian Basins have not yet led to economic success (Brix & Schultz, 1993; Hamilton et al., 2000). Mainly explorationists are of opinion that the Miocene and Pliocene geodynamics of these intramontane basins do not provide viable source rocks; nevertheless, several wells have evidence of gas shows (Hamilton et al., 2000).

The spreading of the Earth's crust in the form of rifting is a highly effective way to accommodate considerable volumes of sediments. Together with normal faulting and sediment stacking, the mechanism often contemporaneously produces dome-shaped closures, a feature of highest interest for hydrocarbon explorationists. Once the extension is followed by compression, the result is an inverted rift system, another setting often considered as a proven, highly prolific exploration concept (Qiang & McCabe, 1998; Branquet et al., 2002; Guiraud et al.,

2010; Roberts & Bally, 2012). A similar fault-near-fault pattern is additionally recognized around inverted normal faults (Bulnes & McClay, 1998; Kossow & Krawczyk, 2002; Shiner et al., 2004), but can also be assigned to planar normal faults accompanied by a similar anticline-shaped closure, known as reverse drag (e.g., Grasemann et al., 2005). An earlier study of the margin of the south-eastern ES sub-basin (Spahić et al., 2011) concluded that the accommodated basin-bounding fault is a finite shape fault with a developed anticline-shaped reverse drag in the hanging wall and a syncline-shaped footwall. Latest study from Häusler et al., (2014) of the St. Margareten fault indicates that the Master fault has listric shape although there is no ductile footwall that could mechanically support this claim. Furthermore, neither the precise timing of the deformations, nor the petroleum systems were the goals of these earlier investigations.

This paper presents a combination of the two quantification methods used for the characterization of an unproven ES petroleum system. By characterizing the opposite margins of the ES basin, initially (i) palinspastic and forward chronologic deformation modelling of the margin of south-eastern basin was performed, and (ii) 1D basin thermal modelling of a single depocentre accommodated along north-western fault-controlled basin boundary. As a result, we elucidate the effects of the multiphase Tertiary deformation events on the main petroleum system elements (PSE) was elucidated and the trap formation time was characterized.

2. EISENSTADT-SOPRON BASIN

The investigated petroleum system is located in the Eisenstadt–Sopron mini-basin, regarded as a subordinate appendix basin separating the Vienna and Pannonian systems (Fig. 1). The main Vienna Basin is a product of the Miocene lateral extrusion moving a large Alpine–Carpathian crustal block northwardly (Decker & Peresson, 1996). Located southeast from the Vienna Unit, the Eisenstadt–Sopron sub-basin was most probably developed above a crystalline basement (Brix & Schultz, 1993; Hamilton et al., 2000), still in near lateral contact with the neighbouring Central Austro-Alpine Zone.

The initiation of the Palaeogene–Tertiary Basin dates to the Late Oligocene–Early Miocene, the time of the post-compressional gravitational collapse (Sclater et al., 1980; Tari & Horváth, 1995). While in the NE, the Late Eggenburgian–Early Ottnangian (20–19 Ma) deposition occupied only the central sections of the Vienna Basin (e.g., Strauss et al., 2006), the realm of the ES Basin interfaced the magma-producing Pannonian region (Szabó et al., 1992). Still no magmatic event has been observed within the Basin. Synchronously, the crustal extension induced propagation of the main bounding faults, triggering the formation of a half-graben and stacking of the fault-adjacent sediment. Initially, at about 17 Ma, the first ingressive waters were followed by fluvial and deltaic environments in the Ottnangian and the Karpatian, presented by the Branderberg Formation (Schönlaub et al., 2000; Kroh et al., 2003). Near the end of the Ottnangian, the transtensional pull-apart opening and transgression onset occurred in the central Vienna Basin (Kováč et al., 2004). Here, extension-controlled subsidence dominated in the western parts of the basin (the Mattersburg Depression) reaching the maximum subsidence and sediment infill of over 2,500 m in the Early Badenian (Kroh et al., 2003). In the eastern–south-eastern part, alongside the Sopron Hills, the Badenian sediments thinned and ended towards the north, while the younger sediments of the Badenian up to the Pannonian extended to the borders of the basin (Fig. 1b). The Lower Badenian is presented by the shallow water carbonate deposition of the famous Leitha limestone succeeded by a clastic deposition (Wiedl et al., 2012). Ceased or slowed, the Badenian subsidence triggered in the Sarmatian a large-scale shallow clastic deposition, predominantly a deltaic type basin infill. After a hiatus, the new depositional phase ceased at the end of Pannonian time. Initiation of an inversion of the basin (Decker et al., 2005) triggered an early and rapid Pliocene desiccation of the main Vienna Basin (Steininger & Wessely 2000), eventually exposing the investigated depositional sequence to a terrestrial event lasting to the present day.

2.1. Geology of the outcrop

The ES mini-basin is characterized by numerous surface lineaments (Häusler et al., 2010), representing the along-strike traces of intrabasinal fault structures. The first of the two investigated large scale faults is associated with the eastern margin of the Eisenstadt–Sopron sub-basin. A near-surface large-scale normal fault (Master fault or MF in figures 1b and 2) is defined by the N–S trending extensional Rust–Fertőrákos system (Grachev & Mukhamediev, 2010). The MF and nearby markers are partially exposed within the abandoned gravel pit shown in figure 2a. The MF dips under 60° towards the west (Decker & Peresson, 1996), displacing the older Badenian calcareous sediments (mostly limestone and marls) in the east, against the west-oriented younger members presented by Sarmatian and Pannonian gravels and calcareous sands (Härzhauser & Kowalke, 2002). The exposed arcuate

hanging wall (Sarmatian) is crosscut by numerous secondary normal synthetic and antithetic faults, including deformation bands (Fig. 2b). For a detailed structural interpretation of the outcrop, see Exner & Grasemann (2010) and Spahić et al., (2011). Beside the outcrop data, a shallow well (up to ≈90 m in depth) drilled in the middle of the gravel pit terminates in Sarmatian clastics (Fig. 2c). However, cuttings of the Badenian limestone present in the vicinity of the shallow borehole bottom may indicate the possible presence of the Badenian in the deeper sections below the investigated outcrop. Here, the early observations were used to characterize the accommodation time of the deformations.

The main goal of the combined surface and subsurface investigations was to index the timing of deformations and evaluate their influence on the key elements of the petroleum system (Magoon & Dow, 1994). Thus, a derived chronological concept was imposed on the key features controlling the subsidence of the basin, such as the Forschenstein fault. A model of a petroleum system understands the processes of hydrocarbon maturation, fluid migration, and entrapment, depicting a system of source rocks, conduit bed, reservoir, and seal (Aydin, 2000, Magoon & Dow, 1994).

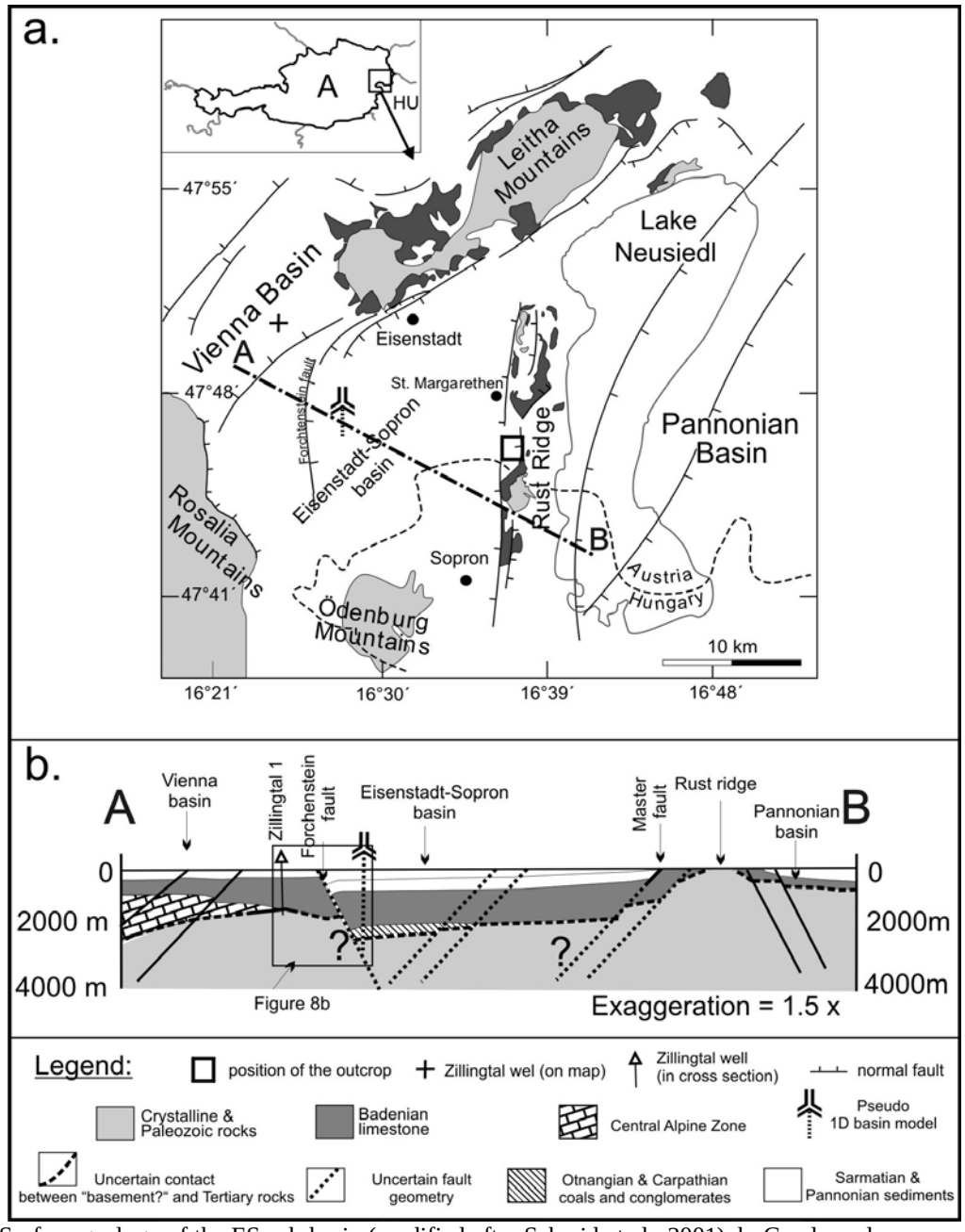

Figure 1. a. Surface geology of the ES sub-basin (modified after Schmid et al., 2001). b. Condensed cross section roughly perpendicular to the East–West basin axis (modified by Brix & Schultz, 1993). The asymmetric mini-basin is accommodated above the crystalline basement; there are no well data within the main depocentre. The geological cross section illustrates the position of the well Zillingtal 1, the 1D numerical maturity models and the main investigated faults.

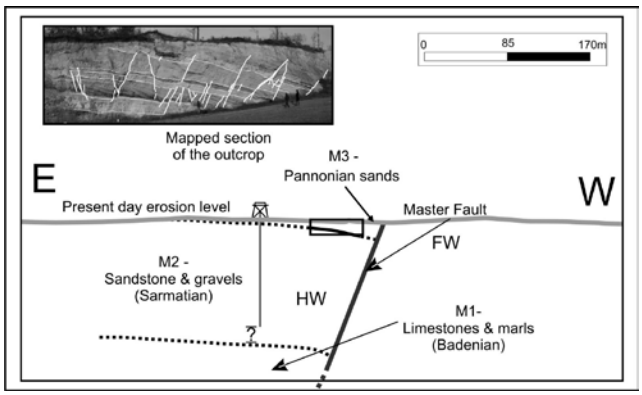

Figure 2. Schematized E–W cross-section of the investigated outcrop, the geology was compiled with the geological map of Austria, sheet Rust, 1: 50.000 (Häusler et al., 2010) and the structural data were collected from observations of the outcrop (Spahić et al., 2011).

3. COAL MINI-PETROLEUM SYSTEM

Brix & Schultz (1993) evaluated the ES mini-basin as a low hydrocarbon prospectivity feature. The size of this triangle-shaped, spatially confined basin feature is ≈ 30 × 30 Km, indicating that an eventual mini-petroleum-play has a rather limited hydrocarbon potential controlled by a typical asymmetric, fault-controlled geometry (Fig. 1b). The authors excluded an oil-generation potential because of the crystalline basement (instead of Alpian Units) positioned below the main Tertiary Formations. Moreover, the total petroleum system is confined to a single coal-dominated methane prone play, additionally emphasizing a lack of anticline-shaped closures. The low hydrocarbon exploration potential is additionally explained by the absence of a source rock system, blaming the crystalline basement located underneath the main Tertiary strata instead main Alpine units.

Nevertheless, it is assumed here that the Ottnangian deposits (17 Ma) presented by the limnic–fluvial, coal-bearing, and delta fan deposits of the Brennberg Series (Dudko et al., 2000) could be considered as the main pod of the source rock interval (Fig. 3). The fault-adjacent wedge accommodated the source rock-reservoir-overburden system of Ottnangian–Karpatian age, where the Badenian marl is considered as a potential seal system. As mentioned earlier, several gas shows have been confirmed in a few wells (Hamilton et al., 2000).

4. METHODOLOGY

Nowadays, a lack of good quality subsurface visualization is often compensated by outcrop observations and the common practice of balancing conceptual models (Heally et al., 2004; King et al., 2010; Sapin et al., 2012; Tearpock & Bischke, 2003) including methods allowing a better understanding of subsurface fluid distribution and properties such as 1D, 2D and 3D modelling of basin and petroleum systems (Hantschel & Kauerauf, 2009).

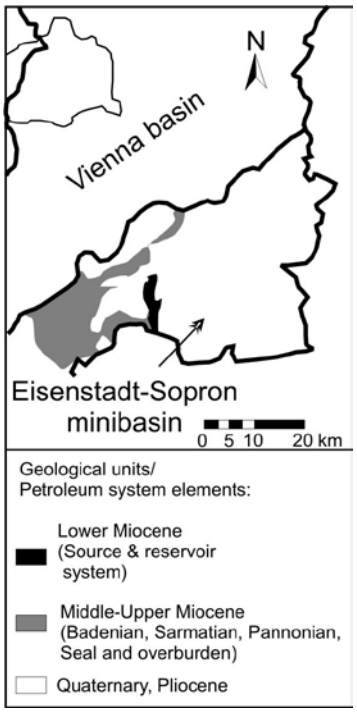

Figure 3. Sketch of the surface distribution (outcrops) of the main elements of the hypothetical petroleum system across the Eisenstadt–Sopron mini-basin. Lower Miocene sediments (black colour) lying below the main Middle Badenian sequence (grey colour) (modified after Hoelzel et al., 2010).

In this contribution, initially palinspastic characterization allowed 2D cross section forward modelling. Subsequently, the 1D thermal basin-modelling method included the amount of the eroded sediments, as well as deeply buried early depositional stages (e.g., the Karpatian and Badenian deposition)

In this contribution, initially palinspastic characterization allowed 2D cross section forward modelling. Subsequently, the 1D thermal basin-modelling method included the amount of the eroded sediments, as well as deeply buried early depositional stages (e.g., the Karpatian and Badenian deposition).

4.1. 2D cross-section balancing

To delineate the exact chronology of the faulting and associated marker deformations as the most probable time of hydrocarbon trap formation, 2D geomechanical-based forward modelling over the MF planar feature (Spahić et al., 2011) accommodated as a basin-bounding fault surface (Fig. 2). For this purpose, the Dynel 2D Schlumberger commercial code was used; see Maerten & Maerten

(2006) for details. The code is based on the finite-element method of mass and momentum conservation allowing restoration, computation of internal forces, forward modelling, and pure shear-based decompaction of sedimentary layers.

The geometry and the geology of the outcrop and its surroundings were extrapolated in a regional 2D composite section (Fig. 2c). The MF was represented by a discontinuity displacing the observed sedimentary sequences. The Badenian, Sarmatian and Pannonian sequences were divided into three homogeneous packages with the same finite element mesh characteristics (Fig. 4). The bedding interfaces were tested allowing and restricting interaction between the layers. In order to observe the mechanical interaction between the layers, the beds were additionally tested for interbedding slip. The left and the right side of the models were free surfaces, qualifying restorations as plane-strain models with no material motion in or out of the cross-section plane. The restoration process sequentially removed stepwise one by one the sedimentary packages starting from the youngest or Pannonian age up to the top of the Badenian surface, additionally calculating the pure-shear strain based decompaction with the level of the palaeowater depth set to ≈150 m.

4.2. Boundary conditions

The MF could slip with friction up to the palaeosea bottom (depositional topography) or target line. The target is presented by a traction free surface that accommodates the displacement during the restoration. Each node of a horizon representing a boundary between sedimentary layers needs to displace a target line (here horizontal), allowing all other nodes to move until equilibrium is attained. As the deposition was interrupted by one or more erosional events, simple restoration of the eroded quantity was calculated by extending the MF in accordance with the dip measurements, paying attention to potential thickness variations. The resulting geometrical quantification of the eroded thickness was minimum 150 m.

4.2.1. Lithological constrains

The investigated Miocene sequence consists of Pannonian sands, interbedded Sarmatian sands, sandstones and poorly consolidated gravel and the Badenian limestones and marls. To observe regional-scale relationships among fault displacement, geometry, and stress, we neglected the sedimentological heterogeneities that were observed in the outcrop were neglected and the physical properties of the rock were simplified into two dominant litho-types: sandstone and limestone. The behaviour across the Pannonian sand layer was disregarded (no deformations were observed at the outcrop); therefore, just for the purposes of pure shear decompaction of the structurally lower layers, the Pannonian lithology was changed to sandstone. The mechanical properties for different lithologies were chosen from the literature and applied to the different model lithologies. For example, for sandstone, the Poisson's ratio used was 0.24 and the Young's modulus was 2.2. For the Badenian limestone, the Poisson's ratio used was 0.25 and Young's modulus was 48. The elastic properties were chosen as the average values of the aforementioned rock types (Drucker & Praeger, 1952). The employed density was the 2D default: 2500 kg/cm^3 for limestone and 2480 kg/cm^3 for sandstone. Note that neither incompetent rheologies, such as salt, nor large homogenous thick clay packages were observed within the region. Therefore, the thin-skinned extension models based on incompetent footwall behaviour, and referred to as "rafting model" (Krészek et al., 2007) were not taken into consideration.

4.2.2. Zero stage (input geometry) for 2D modelling

The present day near-fault geological observation indicated a diversity of processes influencing the finite shape of the outcrop. to understand temporal behaviour of the fault and marker, two key parameters depicting the fault activity were monitored - the sarmatian and the pannonian thicknesses in the hanging wall and their presence/absence within the footwall (Fig. 4).

The simulation set assumed that the mf was active during the sarmatian and the pannonian. Within the zero models, a rust ridge was imposed as an elevated feature protruding already in the sarmatian. Consequently, the deeper positioned sarmatian and pannonian layers in the hanging wall were thickening, unlike those in the footwall. Note that the scenario with a higher fault dip angle (≈70°) (Fig. 4b) was additionally tested.

4.3. Thermal 1D basin modeling

To evaluate hydrocarbon potentials of this minicoalplay, the thermal evolution of the Basin was reconstructed by extrapolating the regional geology data with the thicknesses and lithostratigraphy taken from Well Zillingtal 1 into the 1D pseudo-well (Fig. 1) basin model. For modelling we used commercial software PetroMod Schlumberger (Hantschel & Kauerauf, 2009). Main input data, thicknesses, age of events, erosion, etc are in table 1. The layers thicknesses are combinded with the mini-basin

sequences taken from the regional cross section compiled by Brix & Schultz (1993) (Fig. 1b) and the chronostratigraphical chart from Schönlaub et al., (2000). In this manner, the lithological differences (i.e., the main syn-rift burial-related facial differences) between the hanging wall and the footwall around the key extensional structure (the Forchtenstein fault, Fig. 1) were extrapolated. Within the PetroMod, the upper thermal boundary, presented as the sediment/water interface, was set at 48° northern Europe, calculating the historical to present day sediment/water interface temperature. The Post-Ottnangian intermittent sea-level changes were approximated by extrapolating the palaeowater depth or change in the temporal palaeobathimetric history. The basal heat distribution is discussed in Chapter 5.2.

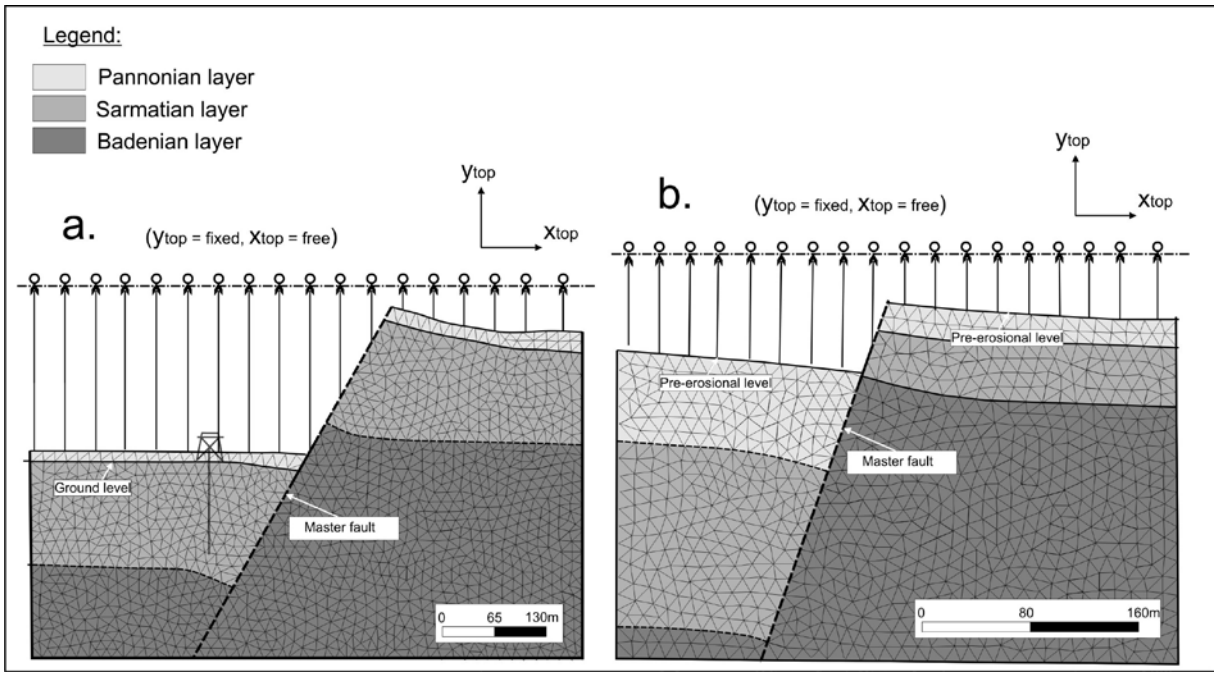

Figure 4. 2D pre-erosional configuration (zero stage) of both the conceptual models discretized in a finite element modelling mesh. Both concepts were tested for bedding interferences and different finite configurations. Finite-element mesh characterized by homogeneous properties for all three layers, sandstone (Pannonian), sandstone (Sarmatian) and limestone (Badenian), The Master fault dip was 60° within both the main conceptual models. a. Planar fault model around the Master fault with the markers. b. Planar fault with unequal sedimentation on the hanging wall and the footwall having an inclination of ≈70°.

Table 1. Input data for the 1D pseudo model of the Eisenstadt-Sopron depocenter.

Layer	*Top [m]*	*Base [m]*	*Thick. [m]*	*Eroded [m]*	*Depo. from [Ma]*	*Depo. to [Ma]*	*Eroded from [Ma]*	*Eroded to [Ma]*	*Lithology*	*PSE*	*TOC [%]*	*Thermal Conductivity*		*Hi [mgHC/g TOC]*
												[W/(mK)] at 20 ℃	*[W/(mK)] at 100 ℃*	
Pannonian	0	45	45	150	11.6	8	8	0	Sandstone [typical]	None		3.95	3.38	
Sarmatian	45	250	205		12.7	11.6			Sandstone [clay rich]	Overburden rock		3.35	2.95	
Upper Badenian	250	1000	750		13.3	12.7			Limestone [ooid grainstone]	Overburden rock		3.00	2.69	
Lower Badenian	1000	2200	1200		15.9	13.9			Marl	Seal rock		2.00	1.96	
Karpatian	2200	2300	100		17	15.9			Sandstone [wacke]	Reservoir rock		2.60	2.40	
Ottnangian	2300	2350	50		17.3	17			Coal [with impurities]	Source rock	50	1.00	1.22	
Basement	2350	3000	650	500	250	200	200	17	Basement	none		2.40	2.25	230
						250								

5. RESULTS AND DISCUSSION

To analyse the main processes within the hypothetical mini-petroleum system controlled by the Forchenstein fault, initially a kinematic forward model was performed using available regional data and outcrop interpretation from the opposite basin side (Figs. 1 and 2). A few wells along the north-western basin margin provided lithological data, whereby for the calibration of the thermal history, present day measurements from Lenkey et al., (2002) were employed.

5.1. Deformation chronology

In order to characterize the chronology of the deformations that controlled the evolution of the coal bearing mini-petroleum system, the results of retro-deformation (restoration) of the south-eastern basin margin and further elaborations in a few main post-rift increments were used. As this basin side does not contain thick syn-rift packages of Karpatian coals (Brix & Schultz, 1993), the post-Badenian deformation chronology could be modelled exclsivly. Thus the forward interpretation begins from Badenian calcareous bed towards the Pannonian layer (the zero stage or present day geometry in Fig. 4a and b).

The pre-restored section length (Pannonian layer) is 3 to 15 % longer than at the beginning of its own deposition (end of the Sarmatian time). The fact that no balancing mismatch was associated with planar fault geometry scenarios gave credibility to the stress computation and subsequent discussion.

The most prominent observation within the modelling results of the south-eastern margin is the fault plane rotation or gentle sloping of the MF fault plane. The 2D model geometry at the end of Sarmatian time captures the counter clockwise rotation of the MF plane (>10°). If the restoration targets presented as a flat line correctly represent the assumed palaeosea bottom, the resulting node equilibrium imposes rotation of the MF plane. A fault plane rotation is one of the key processes responsible for the progressive development of reverse drag (Exner et al., 2004; Gomez-Rivas et al., 2007).

5.1.1. Trapping time: the age of the reverse drag and footwall uplift

The purpose of calculation of the perturbed stress field (relationship Coulomb shear stress and secondary faults) was to predict the exact timing of the secondary deformations crosscutting the outcropped hanging wall (Fig. 2b). Once the computed high stress field was in accord with the observed secondary faulting, a particular increment would disclose the exact timing of the deformations. Thus, for each sensitivity model, or restoration step, the perturbed elastic stress field was calculated, whereby the focus of the interpretation was on criteria for discontinuity prediction. Derived from Coulomb failure criterion, the maximum Coulomb shear stress (MCSS) is a well-known parameter for fault positioning in elastic rock behaviour (Gabrielsen & Koestler, 1987; Maerten et al., 2002; Bahat et al., 2005; Maerten & Maerten, 2006). The friction angle of sand was set at 31° and the fault dip angle at 60° (matching the field observations). The Coulomb failure criterion predicts the maximal vertical stress (σ_{max}). If the fault dip is a function of (i) conjugate intersecting failure planes, (ii) the angle of friction including the (iii) the orientation of the maximum and minimum principal stresses, then the maximum Coulomb shear stress or force causing rock failure could present a potential fault. Henceforth, the maximum Coulomb shear stress is employed as an indicator of the fault density (Maerten & Maerten, 2006):

$$MCSS = \left[\frac{(\sigma_{\max} - \sigma_{\min})}{2}\sqrt{1+\tan^2\varphi}\right] - \tan\varphi\left[\frac{(\sigma_{\max} - \sigma_{\min})}{2}\right] \quad (1)$$

where φ is the friction angle. The code delivers the computed Coulomb shear stress as a colour attribute map. By combining shear stress with a failure criterion, we superimposed the predicted and the real secondary fault locations. Since the code considers no far-field stresses, the change in stress field is a direct result of the force necessary to restore the curved hanging wall and footwall markers. Furthermore, the finite-element models of Grasemann et al., (2003) demonstrate that a reverse drag type is independent of a kinematic vorticity number (i.e., far-field stresses).

The palaeoperturbation shear stress analysis was confined to the Sarmatian increment (zero model in Fig. 4a) because this was the activation period of the regional fault (Decker & Peresson, 1996), wherein the computed high shear stress was in accord with the outcrop-observed secondary normal faults. The resulting Sarmatian shear stress attribute map (a single backward step plotted over the present day section geometry) exhibited a variable shear stress field across the hanging-wall and footwall of the MF (Fig. 5a). The magnitude of the perturbation stress field was several times higher in the hanging wall than within the footwall; nevertheless, the positive shear stress values were mathematically measurable within the footwall. The maximum positive shear stress values were localized in the hanging wall

(Sarmatian) close to the MF but were not very close to the target, indicating no effect of the free surface. As illustrated in figure 5, the positive high–shear stress field directly corresponds to the area of the hanging wall characterized by the cluster of secondary faults observed within the outcropped footwall. Additionally, the orientation of the two shear failure planes derived from the computed stresses over the outcrop area (Fig. 5a) were plotted. The geometry of the displayed shear planes followed the geometry of secondary faults, whereby the size of the failure plains was proportional to the value of the computed MCSS value (see the small rectangle in Fig. 5a).

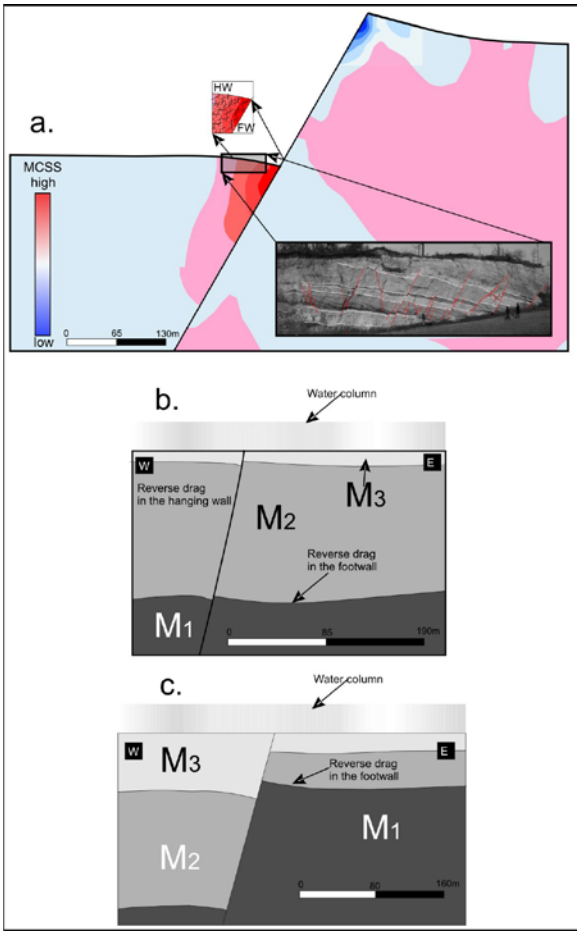

Figure 5. a. Palaeostress distribution around the MF at the end of Pannonian time (MCSS). There is no geometric discrepancy or mass disequilibrium. The exhibited isocontours are a presentation of the computed σ_{xy} or Coulomb shear stress (MCSS). b, c. Restored cross sections (end of the Pannonian) having different stratigraphy-sedimentation rate/erosion zero conditions within the HW and the FW. M1 – Badenian limestone, M2 – Sarmatian sandstone and M3 -Pannonian sandstone. b. Restored Pannonian stage covering both the hangingwall and footwall c. Syn-deformation thickness difference of the Sarmatian and Pannonian layers. Sarmatian extension increased the down lift of the hangingwall and upwards bending of the footwall marker.

For the purpose of the characterization of additional fault activity and the quantification of the footwall uplift as an additional indicator of the trapping time, the fault activation time was fine-tuned and tested by imposition of the real and restored thicknesses in the hanging wall and footwall. The MF activity was assigned to the late Sarmatian and a subsequent hiatus (Härzhauser & Kowalke, 2002) to the Pannonian age. The results indicated a high extensional slip, which induced a relatively higher amount of vertical offset (Fig. 5b and c). The extension-related depression and bending of the hanging wall (higher hanging-wall thicknesses) and the syn-sedimentary footwall uplift ceased at the end of the Pannonian age. After the Pannonian time, the footwall was further exposed to denudation processes; this time resulting in thinner Sarmatian (M2) and Pannonian (M3). The scenario indicates that the increased footwall uplift was mainly extensional in origin (reverse drag) but could also be affected by the postextensional vertical motions. The intensity of a footwall uplift in an extensional tectonic setting is mainly the consequence of the numerous mechanisms (Nøttvedt et al., 1995): rifting (McKenzie, 1978), timing and spatial distribution of the thermal perturbations between the crustal and mantle stress–relaxation processes; effect of the rheological structure; rate of extension; characterization of basement faulting; evolution of the geometry of the depositional basin, including changes in palaeobathimetry; quantification of the eroded thicknesses; slip ratio along the main discontinuities; the amount of finite displacement, *etc*.

In the further text, the constraint of Sarmatian timing of the progressive development of the reverse drag was assumed to analyze the migration–accumulation processes.

5.2. Thermal calibration and source rock maturity prediction

As mentioned earlier, the peripheral, north-western boundary of the ES Basin contains a source rock pod approximated to a thickness of 50 m, deposited at a depth of ≈2300 m, see table 1. The hydrocarbon potential of a source rock is roughly evaluated using basic coal-related organic geochemistry facts. The total organic carbon (*TOC*) values for coals can vary significantly; thus, for the purposes of the evaluation of the Branderberg Formation, type III kerogen (typical higher plant organic matter) was assigned, further characterizing the potential having a lower coal limit of 50 % (Macauley et al., 1985). Characterization of the hydrogen index was driven exclusively by the

traditional organic reach deltaic depositional system and was set to accommodate a moderate to high generation potential: ≈230 mg HC/g TOC. Similarly, the kerogen reaction kinetics formula of Pepper & Corvi (1995) for type III kerogen was used.

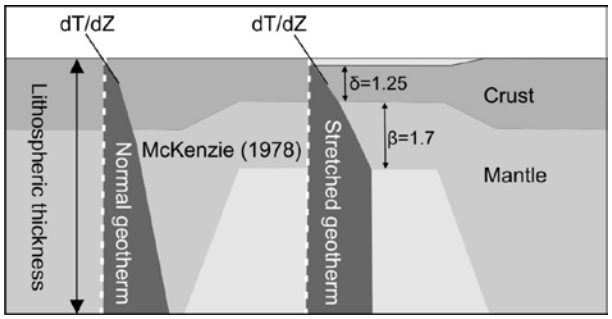

Figure 6. Cartoon of the McKenzie (1978) tectonic model of the lithosphere, before (left), and after stretching (right) (modified after Corver et al., 2009).

The effects of differential basal heating rates of a source rock pod are optimized according to different basin thermal history scenarios. The key processes behind the concept of rift-related exploration are the pre-rift lithosphere geometries and thermal perturbations (Spadini et al., 1997), followed by the initial syn-rift fault-controlled subsidence (syn-rift wedge) and subsequent post-rift sagging (McKenzie, 1978). The calibrated back-stripping analysis and the obtained subsidence curves were fitted to a tectonic model or the basement heat flow history curve. For details of the syn- and post-rift numerical modelling approach, see Baur et al., (2010) and chapter 4.5.1. in Corver et al., (2009). The ES evolution was divided into syn-rift and post-rift cycles (Fig. 6) (Corver et al., 2009), whereby syn-rift presents a period of active extensional faulting in an intracontinental situation (Sclater et al., 1980), encompassing the late Oligocene to the Lower Miocene period.

The post-rift cycle is characterized by thermal subsidence in a continental interior environment from the Badenian to the Pannonian. Initially, the basal heat flow curve of the "McKenzie rifting model" (McKenzie, 1978) having a syn-rift phase from the Late Oligocene to the Early Miocene and a post-rift phase from 20 Ma to the post-Pannonian inversion, or ≈8 Ma, (Tari & Horváth, 1995) was imposed. The syn-rift thermal flux (basal heat flow) ranged within lower thresholds from 59.21 mW/m^2 to 56 mW/m^2 and had a beta-crust stretching factor of 1.25 (δ) and beta mantle of 1.7 (β).

The 1D composite burial–maturity simulations (Fig. 7) performed with the basal heat flow of about 56 mW/m^2 indicated a coal interval entered the main oil window [referred to as easy Ro% by Sweeney & Burnham (1990)] at ≈10 Ma (Fig. 7a), resulting in a present day transformation ratio of slightly over 10%; this is probably not sufficient for the generation of economic hydrocarbon volumes.

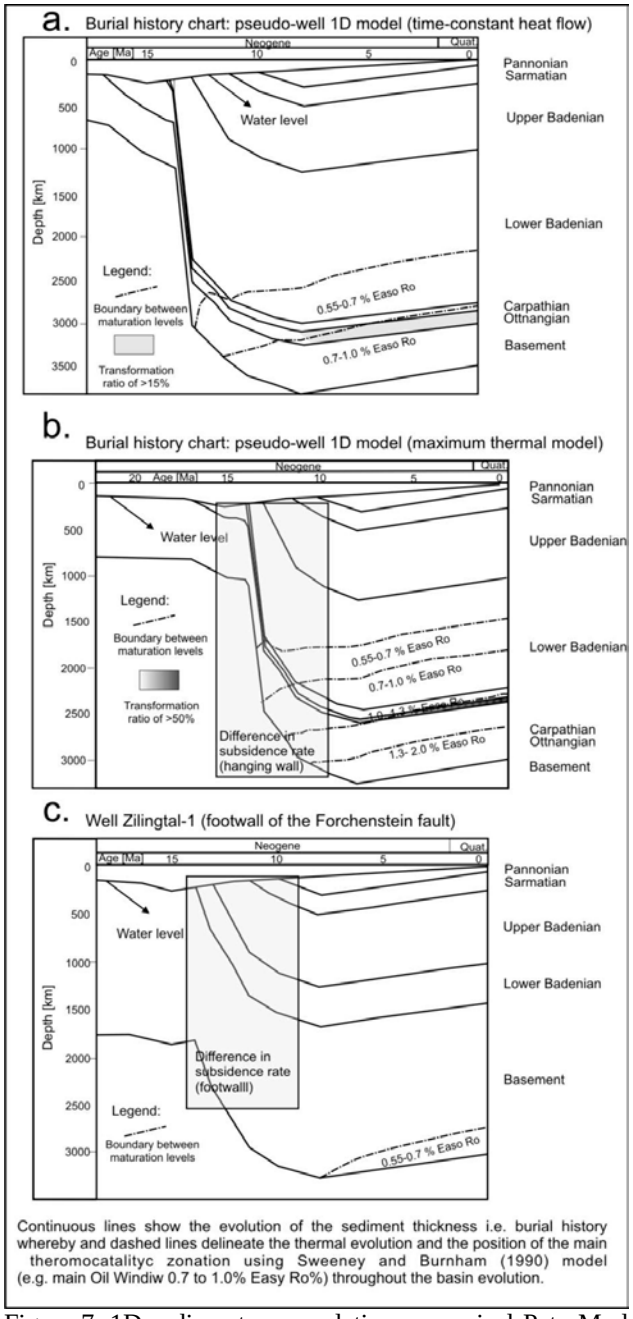

Figure 7. 1D sediment-accumulation, numerical PetroMod 1D models of different thermal and maturation history. a. Extrapolated 1D pseudo well model of the hanging wall area near the Forchenstein fault (time-constant heat flow history model). The results show a low to a satisfactory maturation level with a low Transformation Ratio (TR). b. Same burial history model with the maximum thermal history. The results show a high maturation level of the source rocks and a *TR* of ≈50 %. c. 1D model near the well Zillingtal 1 located at the footwall of Forchenstein fault, no source rocks and no maturation were observed.

By imposing the scenario of the highest thermal history (Fig. 7b), a coal source rock pod would have entered the main oil window 14 Ma ago, allowing satisfactory thermocatalytic fluid burial driven generation (transformation ratio at the present day reaches over 50 %).

On the contrary, the footwall (rectangle area in Fig. 1b) is characterized by a complete lack of a coal source rock system (data from the Zillingtal-1 well), and the area is additionally thermally immature (Fig. 7c). Facies and thermocatalytic difference between the hanging-wall wedge system and the drilled footwall indicates to a downwards rotation of the hanging-wall and an upwards lift of the footwall, dating the Karpatian and Ottnangian times.

5.2.1. A fault-controlled migration-accumulation scenario

According to Landwein (1988), the present day main oil window stretches from 4000 to 6000 m (below the Miocene section of the Vienna Basin, Alpine Units), and the basal heat flow ranges from 50 to 55 mW/m^2. Unlike those in the Vienna Basin, the relatively high thermal flux in Eisenstadt–Sopron was also observed in the adjacent Styrian Basin, another marginal sub-basin of the Pannonian Basin (Dunkl *et al*., 1998). Subsequently, the question of the origin of the mini-basin and the current tectonic systematization arises as to whether the investigated mini-basin is associated with the main Vienna Basin (due to depositional similarity) or whether it is rather deeply rooted as a realm zone in the Pannonian system (Dolton, 2006). In the following discussion, the eventual generation–migration processes are schematized using the scenario of the considerable thermal effect on the source rock system (higher heat flow scenario that was calibrated to the regional heat flow maps and measurements presented in Lenkey et al., (2002).

Generally, discontinuities behave as conduits once near-fault permeability has increased as a consequence of rock deformation (Weber, 1978).As the Forchenstein fault was accommodated before the hydrocarbon expulsion (Fig. 8a), and was already a prominent, adjacent feature during the source rock expulsion, this discontinuity could have played a primary controlling role in the eventual fluid migration. Once the source rocks had generated enough fluid or reached a satisfactory transformation ratio, the fluid (probably methane) vacated the near-fault source rock system. The trap formation time, according to the restoration results, was approximately late Sarmatian and/or Pannonian age. As the expulsion onset commenced much before the trap formation, at ≈14 Ma, the critical moment associated with eventual anticline traps was further shifted to the late Sarmatian or Pannonian time, resulting in 4–5 Ma years of possible non-favourable fluid migration (Fig. 8a). Nevertheless, some of the fluids could have saturated the fault gauge, enabling the spacing for fluid to percolate further towards the low-pressure area or high-porosity niches (Moretti & Deacon. 1995). Eventually, depending of a near-fault lithological juxtaposition and lithology of the overburden layers, a fault-controlled migration could have produce hydrocarbon accumulations in the reservoirs; however, they would have been distributed mainly in the footwall domain (Fig. 8a and 8b).

5.2.2. Footwall traps

From the hydrocarbon exploration perspective, two fault drag effects could be observed: a hanging wall marker downward depression and an increased uplift of the footwall (Resor & Pollard, 2012). From a traditional anticline-related trapping perspective, the critical moment should have been postponed towards either syn-Sarmatian (Fig. 8a, hatched areas) or syn-Pannonian events since such events may produce favourable trapping geometries. However the timing of the footwall trap (Spahić et al., 2013) generation allows a more favourable critical moment - the moment when a petroleum system should function (Fig. 8b). The most prominent and published analogue of the successful fault-related reverse drag petroleum system comes from Venezuela, the Oritupano–Leona block. The large hydrocarbon accumulations, estimated at 2.7 million bbl, were produced from a single trap (Porras et al., 2003).

6. CONCLUSIONS

The presented synthesis and chronology of the processes between the early Tertiary source rock development, the reservoir and the timing of hydrocarbon generation and migration give potentially new conceptual ideas for this underexplored mini-basin.

The Karpatian as a phase of fault-related sediment burial, when a late Sarmatian extension could result in local uplifts in the SE basin margin. Around a depocentre, the Karpatian coal bearing source rock system could enter into an early generation window already during the Badenian. The simulation results indicate that the high heat flow values could further contribute to a satisfactory transformation rate of the coaly organic matter. The main trap formation phase is associated with the terminal phase (Sarmatian/Pannonian) of normal faulting that is associated with reverse drag development.

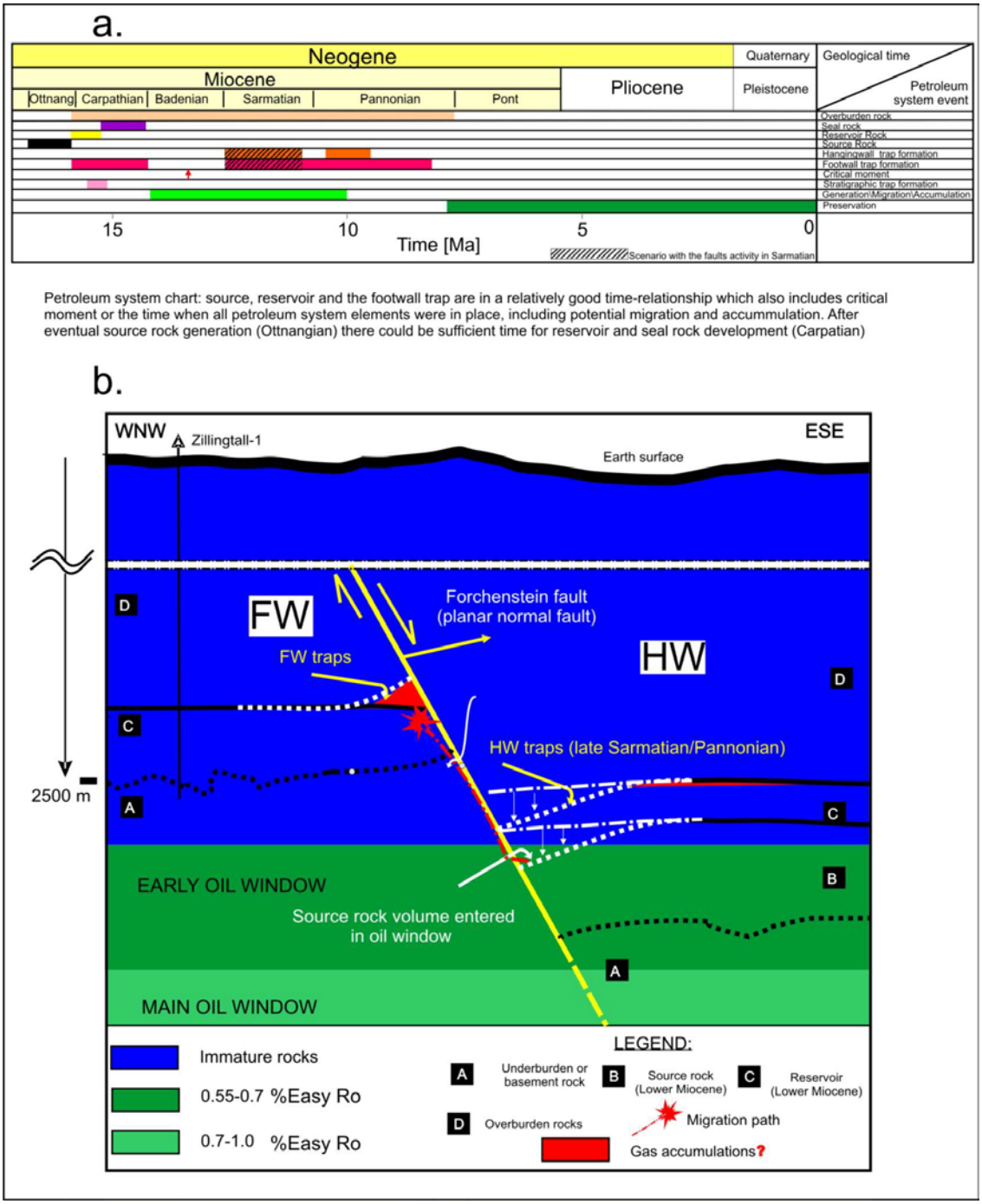

Figure 8. a. Petroleum system chart. b The sketch illustrates hypotetical petroleum system (maturity, migration and eventual accumulations) and possible influence of the reverse drag development in this unproven hydrocarbon play: (i) Reverse drag development and potential source rock maturation (after bending of the strata), (ii) A scenario of the possible fault-related migration–accumulation scenario. The schematized cross section illustrates petroleum system elements near the basin edge (Forschenstein fault). The maturity (main and early oil window) is extrapolated from the results of 1D modelling. One of the major drawbacks could be a lack of seal or cap rock in the footwall area, because Ottnangian clays are captured only in the main depocenter.

The 1D thermal modelling suggests that there is a high probability of active source rocks around a depocentre, however with limited generation volumes and top sealing capabilities.The resulting normal faulting chronology indicated a possibility that eventual hydrocarbon traps could be associated with uplifted fault-adjacent footwall synclines.

Acknowledgements

Many thanks to Dr. Kurt Decker (University of Vienna, Austria) for very valuable critical comments and suggestions on the early version of the manuscript. A part of this study concerning to the stratigraphy of Miocene of Pannonian Basin and its peripheral sub-basins (Lj.R)

represents a result of the project no.176015 supported by Ministry of Education and Science, Republic of Serbia.

REFERENCES

Aydin, A., 2000. *Fractures, faults, and hydrocarbon migration and flow*. Marine and petroleum geology, 17. 797-814.

Bahat, D., Rabinovitch, A. &Frid, V., 2005. *Tensile fracturing in rocks: tectonostratigraphic and electromagnetic radiation methods*. Springer, berlin.

Baur, F., Littke, R, Wielens, H., Lampe, C. & Fuchs, T., 2010. *Basin modelling meets rift analysis–A numerical modelling study from the Jeanne d'Arc basin, offshore Newfoundland, Canada*. Marine and Petroleum Geology 27. 585–599.

Branquet, Y., Cheilletz, A., Cobbold, P.R., Baby, P., Laumoniere, B. & Giuliani, G., 2002. *Andean deformation and rift inversion, eastern edge of Cordillera Oriental (Guateque–Medina area), Colombia*. Journal of South American Earth Sciences. 15. 391–407.

Brix, F. & Schultz, O., (Eds.) 1993. *Erdol und Erdgas in Osterreich*. Museum for Natural History, Vienna, ISBN 3-85028-236-8. (*in German*).

Bulnes, M. & McClay, K.R., 1998. *Structural analysis and kinematic evolution of the inverted central South Celtic Sea Basin*. Marine and Petroleum Geology 15. 667–687.

Corver, M., Doust, H., Diederik van Wees, J., Bada, G. & Cloetingh, S., 2009. *Classification of rifted sedimentary basins of the Pannonian Basin System according to the structural genesis, evolutionary history and hydrocarbon maturation zones*. Marine and Petroleum Geology 25. 1452–1464.

Decker, K. & Peresson, H., 1996. *Rollover and hanging-wall collapse during Sarmatian-Pannonian synsedimentary extension in the Eisenstadt basin*. Mitt. Ges. Geol. Österr. 41. 45–52.

Decker, K., Peresson, H. & Hinsch, R., 2005. *Active tectonics and Quaternary basin formation along the Vienna Basin Transform fault*. Quaternary Science Reviews 24. 307–322

Dolton, G., 2006. *Pannonian Basin Province, Central Europe (Province 4808)* Petroleum Geology, Total Petroleum Systems, and Petroleum Resource Assessment. USGS Bulletin 2204–B.47

Drucker, D.C. & Praeger, W., 1952. *Soil mechanics and plastic analysis or limit design.* Quart Appl Maths 10.157.

Dudko, A., Pistotnik, J., Elecko, M., Vass D, Hok, J., Vozar, J., Nagy, A. & Sefara, J., 2000. *Tectonic map. Danube region Environmental Geology Programme DANREG–Explanatory Notes*. Jahrbuch der Geologischen Bundesanstalt 12.493–504.

Dunkl, I., Grasemann, B. & Frisch, W., 1998. *Thermal effects of exhumation of a metamorphic core complex on hanging wall syn-rift sediments: An example from the Rechnitz Window*, Eastern Alps. Tectonophysics 297. 31–50.

Exner, U. & Grasemann, B., 2010. Deformation bands in gravels: Displacement gradients and heterogeneous strain. J of the Geological Society, London 167. 905–913.

Exner, U., Mancktelow, N.S. & Grasemann, B., 2004. *Progressive development of S-type flanking folds in simple shear*. Journal of Structural Geology 26. 2191–2201.

Gabrielsen, R.H. & Koestler, A.G., 1987. *Description and structural implication of fractures in the Late Jurassic sandstones of the Troll Field, northern North Sea*. Norsk Geologisk Tidsskrift. 67. 371–381.

Gomez-Rivas, B., Bons, P., Griera, A., Carreras, J., Druguet, E. & Evans, L., 2007. *Strain and vorticity analysis using small-scale faults and associated drag folds*. Journal of Structural Geology 29. 1882–1899.

Grachev, F. & Mukhamediev, A., 2010. On the nature of the junction zone between the Vienna and Pannonian sedimentary basins. Izvestiya, Physics of the Solid Earth 46. 849–861.

Grasemann, B., Martel, S. & Passchier, C., 2005. *Reverse and normal drag along a fault*. Journal of Structural Geology 27. 999–1010.

Grasemann B., Stüwe, K. & Vannay, J.-C., 2003. *Sense and non-sense of shear in flanking structures*. Journal of Structural Geology 25. 19–34.

Guiraud, M., Buta-Neto, A. & Quesne, D., 2010. *Segmentation and differential post-rift uplift at the Angola margin as recorded by the transform-rifted Benguela and oblique-to-orthogonal-rifted Kwanza basins*. Marine and Petroleum Geology 27.1040 – 1068

Hamilton, W., Wagner, L. & Wessely, G., 2000. *Oil and Gas in Austria***.** Mitt. Oesterr. Geol. Ges. 92. 235-262.

Hantschel, T. & Kauerauf, A., 2009. *Fundamentals of Basin and Petroleum System Modeling*. Springer. 476.

Härzhauser, M. & Kowalke, T., 2002. *Sarmatian (Late Middle Miocene) Gastropod Assemblages of the Central Paratethys*. Facies 46. 57–82.

Häusler, H., Figdor, H., Hammerl, C., Kohlbeck, F., Lenhardt, W. & Schuster, R., 2010. *Geologische Karte der Republik Österreich 1:50.000, Erläuterungen zu Blatt 78 RUST*. Geologische Bundesanstalt, Wien. (*In German*)

Häusler, H., Scheibz, J., Chwatal W., Kohlbeck, F. (2014)**:** *Coeval Lower Miocene subsidence of the Eisenstadt Basin and relative updoming of its Austroalpine frame: implications from high‐resolution geophysics at the Oslip section (Northern Burgenland, Austria).* International Journal of Earth Sciences (Geol Rundsch). Doi 10.1007/s00531-014-1084-8.

Heally, D., Kusznir, N. & Yielding, G., 2004. *An inverse method to derive fault slip and geometry*

from seismically observed vertical stratigraphic displacements using elastic dislocation theory. Marine and Petroleum Geology 21. 923–932.

Hoelzel, M., Decker, K., Zamolyi, A., Strauss, P. & Wagreich, M., 2010. *Lower Miocene structural evolution of the central Vienna Basin (Austria).* Marine and Petroleum Geology 27. 666–681.

King, C.R., Backé, G., Morley, C.K., Hillis, R.R. & Tingay, M.R.P., 2010. *Balancing deformation in NW Borneo: Quantifying plate-scale vs. gravitational tectonics in a delta and deepwater fold-thrust belt system*. Marine and Petroleum Geology 27. 238–246.

Kossow, D. & Krawczyk, C.M., 2002. *Structure and quantification of processes controlling the evolution of the inverted NE-German Basin*. Marine and Petroleum Geology 19. 601–618.

Kováč, M., Baráth, I., Harzhauser, M., Hlavatý, I. & Hudáčková, N., 2004. *Miocene depositional systems and sequence stratigraphy of the Vienna Basin*. Cour. Forsch.-Inst. Senckenberg 246. 187–212.

Krézsek, C., Adam, J. & Grujic, D., 2007. *Mechanics of fault and expulsion rollover systems developed on passive margins detached on salt: insights from analogue modelling and optical strain monitoring. In: Jolley SJ, Barr D, Walsh JJ, Knipe RJ (eds) Structurally complex reservoirs.* Geological Society of London Special Publications 292. 103–121.

Kroh, A., Härzhauser, M., Piller, W.E. & Rögl, F., 2003. *The Lower Badenian (Middle Miocene) Hartl Formation (Eisenstadt-Sopron Basin, Austria)* In: Piller, WE (ed) Stratigraphia Austriaca. Österr. Akad. Wiss., Schriftenr. Erdwiss. Komm. 16.87–109.

Landwein, H.W. ,1988. *Organic geochemistry of Vienna Basin: model for hydrocarbon generation in overthrust belts*. AAPG Bulletin 72. 586–599

Lenkey, L., Dövényi, P., Horváth, F. & Cloeting, S.A.P.L., 2002. *Geothermics of the Pannonian Basin and its bearing on the neotectonics EGU*. Stephan Mueller Special Publication Series 3. 29–40.

Macauley, G., Snowdon, L.R. & Ball, F.D., 1985. *Geochemistry and geological factors governing exploitation of selected Canadian oil shale deposits*. Geological Survey of Canada. 65.

Maerten, L. & Maerten, F., 2006. *Chronologic modelling of faulted and fractured reservoirs using geomechanically based restoration:Technique and industry applications.* AAPG Bulletin, 90. 1201–1226.

Maerten, L., Gillespie, P. & Pollard, D.D., 2002. *Effect of local stress perturbation on secondary fault development*. Journal of Structural Geology 24. 145–153.

Magoon, L.B. & Dow, W.G., 1994. *The Petroleum System, From Source to Trap*. AAPG Memoir, 60. pp 655.

McKenzie, D., 1978. *Some remarks on the development of sedimentary basins*. Earth and Planet Science Letters 40. 25–32.

Moretti, I. & Deacon, K., 1995. *Subsidence, maturation and migration history of the Tampen Spur area*. Marine and Petroleum Geology 12. 345–375.

Nøttvedt, A., Gabrielsen, R.H. & Steel, R.J., 1995. *Tectonostratigraphy and sedimentary architecture of rift basins, with reference to the northern North Sea*. Marine and Petroleum Geology 12. 881–901.

Pepper, A.S. & Corvi, P.J., 1995. *Simple kinetic models of petroleum formation. Part I: Oil and gas generation from kerogen*. Marine and Petroleum Geology 12. 291–319.

Porras, J.S., Vallejo, E.L., Marchal, D. & Selva, C., 2003. *Extensional folding in the eastern Venezuela Basin: Examples from fields of Oritupano-Leona block*. Search and Discovery Article #50003,7.

Resor, P. & Pollard, S., 2012. *Reverse drag revisited: Why footwall deformation may be the key to inferring listric fault geometry.* Journal of Structural Geology 41. 98–109.

Qiang, J. & McCabe, P.J., 1998. *Genetic features of petroleum systems in rift basins of eastern China*. Marine and Petroleum Geology 15. 343–358.

Roberts, A. & Bally, A.W., 2012. *Phanerozoic rift systems and sedimentary basins*. Elsevier, pp 528

Sapin, F., Ringenbach, J.-C., Rives, T. & Pubellier, M., 2012. *Counter-regional normal faults in shale-dominated deltas: Origin, mechanism and evolution*. Marine and Petroleum Geology 37. 121–128.

Schmid, H.P., Harzhauser, M. & Kroh, A., 2001. *Hypoxic events on a Middle Miocene carbonate platform of the central Paratethys (Austria, Badenian, 14 Ma)*. Ann Naturhist. Mus Wien 102A. 1–50.

Schönlaub, H.P., Heinrich, M., Herrmann, P., Hofmann, T., Koller, F., Kollmann, W.F.H., Lenhardt, W. A., Pahr, A., Piller, W.E., Schermann, O., Schönlaub, H.P., Belocky, R., Seiberl, W., Walach, G. & Zorn, I., 2000. *Erläuterungen zur Geologischen Karte des Burgenlandes 1: 200.000*. Geologische Bundesanstalt: pp 130.

Sclater, J.G., Royden, L., Horvath, F., Burchfiel, B.C., Semken, S. & Stegena, L., 1980. *The formation of the intra-carpathian basins as determined from subsidence data*. Earth and Planetary Science Letters 51. 139-162.

Shiner, P., Beccacini, A. & Mazzoli, S., 2004. *Thin-skinned versus thick-skinned structural models for Apulian carbonate reservoirs: Constraints from the Val d'Agri Fields*, S Apennines, Italy. Marine and Petroleum Geology 21. 805–827

Spadini, G., Robinson, A. & Cloetingh S., (1997): *Thermo-mechanical modelling of Black Sea basin formation, subsidence and sedimentation*. A. Robinson (Ed.), American Association of Petroleum Geologists Memoirs, 68. 19irs

Spahić, D., Exner, U., Behm, M., Grasemann, B., Haring, A. & Pretsch, H., 2011. *Listric versus planar normal fault geometry: An example from the Eisenstadt-Sopron Basin (E Austria).* International Journal of Earth Sciences (Geologische Rundschau) 100. 1685–1695.

Spahić, D., Grasemann, B. & Exner, U., 2013. *Identifying fault segments from 3D fault drag analysis (Vienna Basin, Austria).* Journal of Structural Geology 55. 182–195.

Steininger, F.F. & Wessely, G., 2000. *From the Tethyan Ocean to the Paratethys Sea: Oligocene to Neogene stratigraphy, paleogeography and paleobiogeography of the circum-Mediterranean region and the Oligocene to Neogene Basin evolution in Austria*. Mitt. Oesterr. Geol. Ges. 92. 95-116.

Strauss, P., Harzhauser, M., Hinsch, R. & Wagreich, M., 2006. *Sequence stratigraphy in a classic pull-apart basin (Neogene, Vienna Basin). A 3D seismic based integrated approach.* Geologica Carpatica 57. 185–197.

Sweeney, J.J. & Burnham, A.K., 1990. *Evaluation of a simple model of vitrinite reflectance based on chemical kinetics*. AAPG Bull 74. 1559–1570

Szabó, C.S., Harangi, S. & Csontos, L., 1992. *Review of Neogene and Quaternary volcanism of the Carpathian–Pannonian region*. Tectonophysics 208. 243–256.

Tari, G. & Horváth, F., 1995. *Middle Miocene extensional collapse in the Alpine-Pannonian transitional zone. In: Horváth F, Tari G, Bokor K (eds): Extensional collapse of the Alpine orogene and hydrocarbon prospects in the basement and fill of the western Pannonian Basin*. AAPG Inter Confand Exhib, Guidebook to fieldtrip 6. 75–105.

Tearpock, D.J. & Bischke, R.E., 2003. *Applied Subsurface Geological Mapping*. Prentice Hall PTR. pp 821.

Weber, K.J., 1978. *Hydrocarbon distribution patterns in Nigerian growth fault structures controlled by structural style and stratigraphy.* Journal of Petroleum Science and Engineering 1(2). 91–104.

Wiedl, T., Harzhauser, M. & Werner, E.P, 2012. *Facies and synsedimentary tectonics on a Badenian carbonate platform in the southern Vienna Basin (Austria, Central Paratethys)*. Facies 58.523–548.

Received at: 26. 05. 2014
Revised 12. 08. 2014
Accepted for publication at: 17. 03. 2015
Published online at: 23. 03. 2015